Ships and Offshore Structures

ISSN: (Print) (Online) Journal homepage: www.tandfonline.com/journals/tsos20

Parametric finite element analysis of naturally corroded steel specimens using 3D surface laser scans

Michael Biglu, Franz von Bock und Polach & Sören Ehlers

To cite this article: Michael Biglu, Franz von Bock und Polach & Sören Ehlers (21 Apr 2025): Parametric finite element analysis of naturally corroded steel specimens using 3D surface laser scans, Ships and Offshore Structures, DOI: 10.1080/17445302.2025.2492429

To link to this article: https://doi.org/10.1080/17445302.2025.2492429

Published online: 21 Apr 2025.

SHIPS AND OFFSHORE STRUCTURES
https://doi.org/10.1080/17445302.2025.2492429

Taylor & Francis
Taylor & Francis Group

Parametric finite element analysis of naturally corroded steel specimens using 3D surface laser scans

Michael Biglu[a], Franz von Bock und Polach [b] and Sören Ehlers[c]

[a]National Renewable Energy Laboratory, Golden, CO, USA; [b]Institute for Ship Structural Design and Analysis, Hamburg University of Technology, Hamburg, Germany; [c]DLR Institute for Maritime Energy Systems, Geesthacht, Germany

ABSTRACT

Corrosion is considered a uniform thickness reduction design guideline of the maritime industry. However, additionally, the corroded and irregular morphology of the surface affects the steel's load-bearing capacity and its impact on the strength and elongation behaviour of the steel is not yet fully understood. These effects on the local behaviour of steel structures under tensile loading were investigated with tensile tests on naturally corroded steel specimens and nonlinear finite element simulations including the corroded surface morphology with a uniform surface idealation. The models also include the deformed specimen shape. The developed approach led to highly accurate parametric finite element models predicting the ultimate tensile strength and longitudinal position of fracture. The results show that all included aspects are essential for accurate simulations, while solely the maximum available surface resolution was not as decisive.

ARTICLE HISTORY
Received 25 January 2024
Accepted 3 April 2025

KEYWORDS
Corrosion; finite element analysis; numerical simulation; strength analysis; integrity of steel structures

1. Introduction

Corrosion can lead to complete failure of (steel) structures; offshore structures and ships are especially vulnerable to corrosion. Local corrosion damages can lead to cracks in tanks and the total loss of the vessel. Two catastrophic oil spills, caused by structural failure due to corrosion, occurred when the single-hull oil tankers MV Erika (1999, off the French coast) and MV Prestige (2002, off the coast of Galicia, Spain) broke apart and sank after encountering severe weather (Paik et al. 2003; Garbatov et al. 2014; Zhang et al. 2017). To prevent such events, shipbuilding construction guidelines, developed by organisations such as the International Maritime Organisation (IMO) and the International Association of Classification Societies (IACS), were improved (Paik et al. 2003; IACS 2023a). The IACS is an organisation with twelve member classification societies that sets a minimum technical standard and requirements for the design, construction and compliance of ships throughout their service life. Melchers stated the impact of corrosion on the structural integrity of a hull, as it can lead to material degradation, fatigue crack initiation, brittle fracture, and unstable failure (Melchers 2008). Shipbuilding construction guidelines take into account uniform corrosion additions, depending on the location of the structural element and the related corrosion rate (Saad-Eldeen et al. 2011). Respective structural survey guidelines (Saad-Eldeen et al. 2011; IACS 2023b) recommend replacing certain structural members when the local pitting intensity has exceeded a certain limit due to further strength reduction linked to pittings. Naturally corroded specimens undergo a corrosion process that leads to irregular surface morphology, which may include pitting corrosion – a localised form of degradation characterised by deep, narrow pits – alongside other surface deterioration patterns.

The effects of corrosion on steel – in particular, pitting corrosion – have been investigated for more than a decade. By nature, corroded surfaces are not uniform and are therefore challenging to investigate accurately. A widely applied approach is to perform tensile tests with corroded tensile test specimens, with either naturally corroded surfaces or artificial pittings (Paik et al. 2004). The conclusions are that pitting corrosion leads to a reduction in tensile strength (Appuhamy et al. 2011; Kaita et al. 2011; IACS 2023b) and breaking strain (Yao et al. 2018; Garbatov et al. 2019; IACS 2023b). However, as it was often not possible to distinguish precisely between different geometric parameters, the actual causes of these effects are not fully understood. Also, with respect to conducted finite element simulations many simplifications were applied because of the missing availability of accurate surface scan data and the limited capabilities of the hardware at that time. This is now changing due to more advanced scanning and increased computational power.

Finite element simulations are widely used in evaluating the residual strength of structures, including the strength of corroded steel structures. Studies in the 2000s already conducted finite element analysis (FEA) to investigate the effects of corrosion (Paik et al. 2003). Although the pittings were artificially created and evenly distributed, the prediction of ultimate compressive strength is expected to be valid for randomly distributed pitting corrosion. This was verified by means of a nonlinear finite element calculation with ANSYS (Paik et al. 2003).

A common approach is to account for the corrosion damage by uniformly reducing the plate thickness or by simplifying pitting corrosion with, e.g. spherical or conical geometries. Zhang *et al.* performed a nonlinear finite element ultimate strength analysis for pitting corroded plates, idealising the pittings with a conical or spherical shape with the same corroded volume loss as the actual pits (Zhang et al. 2016). In particular, they concluded that the reduction in ultimate strength is relative to the volume loss (Zhang et al. 2016).

CONTACT Franz von Bock und Polach franz.vonbock@tuhh.de

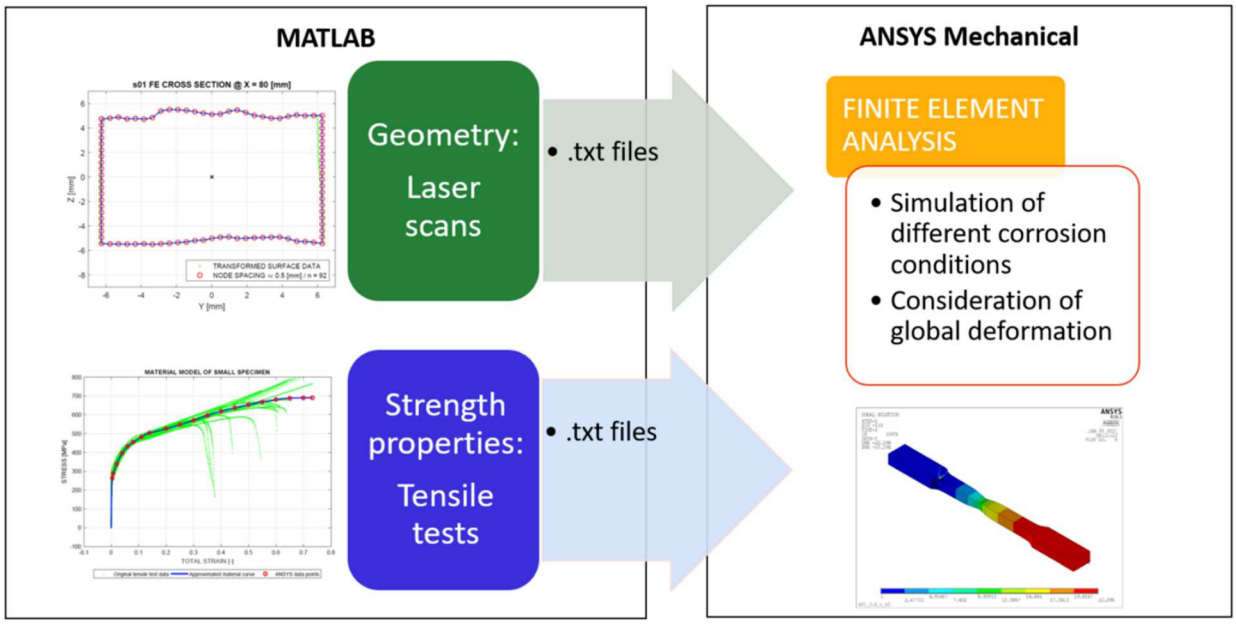

Figure 1. Numerical modeling approach for corroded specimens (This figure is available in colour online).

Rahbar-Ranji studied the effect of surface roughness on the plastic collapse load of corroded steel plates. Using nonlinear FEA with ANSYS of simply modified finite element models, he found that the strength reduction factor increases almost linearly with increasing surface roughness. He concluded that the assumption of uniform thickness can lead to a 5% overestimation of the plastic collapse load and a 3.5% reduction factor in buckling strength for a uniform surface (Rahbar-Ranji 2012). Other FEA studies by Rahbar-Ranji on stiffened plates with pitting corrosion concluded that the strength reduction factor increases with the ratio of pitting depth to thickness and that this observation does not appear to be related to plate thickness, Degree of Pitting (DOP), or the shape or size of the stiffeners (Rahbar-Ranji et al. 2015). However, it was observed that the magnitude of the reduction was correlated with the plate thickness (Rahbar-Ranji et al. 2015).

A group of researchers, including Garbatov, Guedes Soares, and Saad-Eldeen, performed several studies on the effects of corrosion using a corroded specimen of a box girder (Saad-Eldeen et al. 2011; Garbatov et al. 2014; Garbatov et al. 2016). They concluded that the assumption of uniform corrosion by reducing the average thickness is not accurate enough, as changes in mechanical properties influenced their experimental results. Kim *et al.* measured the residual thickness of naturally corroded steel specimens and carried out tensile tests (Kim et al. 2017). They suggested an effective thickness formulation based on the mean and standard deviation of the residual thickness.

In contrast to early researchers who focused on simplifying the corroded morphology (both in numerical finite element analysis and in real experiments), more and more researchers are performing detailed numerical analyses based on direct laser surface scans (Ahmmad and Sumi 2010; Appuhamy et al. 2011; Kainuma et al. 2014; Wang et al. 2017). In studying the location of the fracture of a corroded specimen, it was found that the location of the fracture cross section is not correlated with the minimum thickness, and it was assumed that other parameters, e.g. pitting distribution and shapes, also have an impact (Garbatov et al. 2019; Tekgoz et al. 2020). Therefore, the effects of corrosion on the behaviour of steel cannot be correlated only with volume loss or changes in cross-sectional area (Tekgoz et al. 2020). Other studies have confirmed that surface roughness and respective pitting have significant effects on the residual strength of corroded steel elements due to local stress concentrations (Nakai et al. 2004; Kariya et al. 2005; Ahmmad and Sumi 2010; Ahmad 2012; Rahbar-Ranji 2012; Rahbar-Ranji et al. 2015); therefore, the corroded surface morphologies are influencing the strength behaviour and consequently must be adequately considered in finite element simulations. The disadvantage of morphological simplifications of the corroded surface, e.g. reduced resolution of pitting, is that the studied effects of

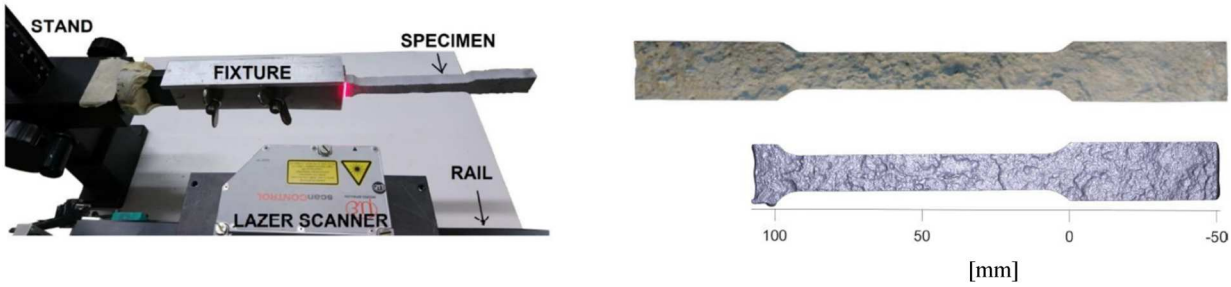

Figure 2. Laser scanning setup and surface scan compared with photograph of real corroded surface (Neumann and Ehlers 2019). The scale on the right below the specimen shows the longitudinal coordinates in millimeter (This figure is available in colour online).

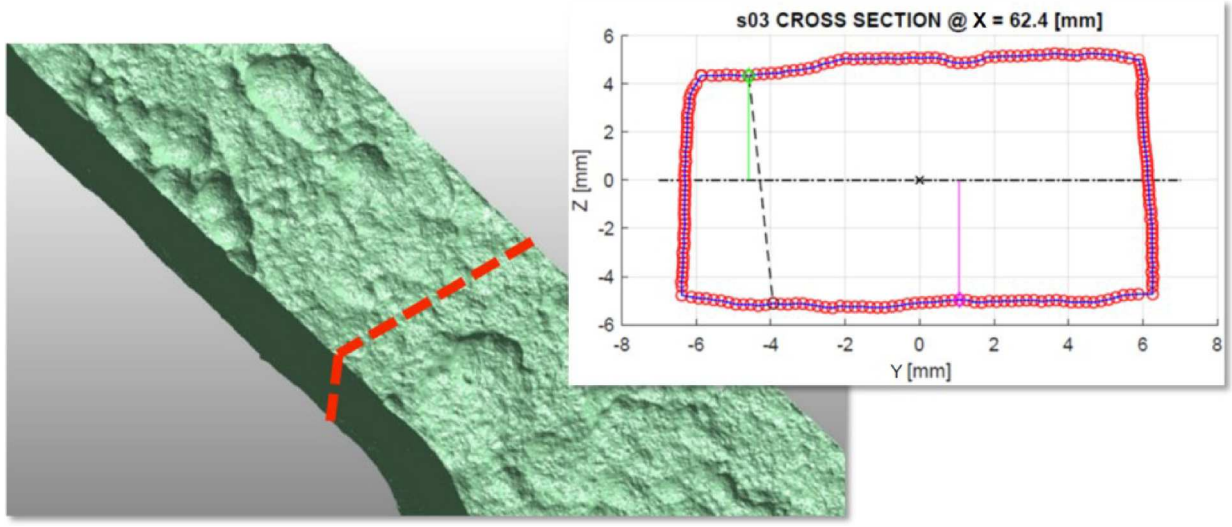

Figure 3. Example of resulting sample geometry and extracted cross section. Right chart: Coloured lines show the minimum distances measured from centreline (horizontal dashed line) to surface. The vertical dashed line represents the minimum thickness in the cross section (This figure is available in colour online).

corrosion on mechanical properties are significantly influenced by the simplification of the corroded morphology (Wang et al. 2017). Moreover, the conditions of application are not described in detail; the empirical factors especially seem to be arbitrary in most cases, and the applicability has not been recognised on a large scale (Wang et al. 2017). Park *et al.* investigated numerically and experimentally corrosion damage on cylindrical ring-stiffed submarine pressure hulls (Park et al. 2024). Their results showed that the residual strength was reduced by up to 12.1% compared to intact condition. Corrosion was considered as artificially machined down circles, leading to local material reductions between 13.3% and 25%.

A comprehensive work by Wang *et al.* studied a corroded steel specimen under tensile loading. The top and bottom surfaces were scanned and modelled in finite element models (Wang et al. 2017). They concluded that the ultimate load is mainly affected by the thickness loss while the deformability degradation is related to the local volume loss. In addition, most of the specimens broke near the minimum cross-sectional area (Wang et al. 2017). Although the effects of pitting corrosion have been studied for decades, the actual influences have not yet been conclusively determined (Wang et al. 2018). In experimental and numerical finite element studies, pitting corrosion is often simplified by artificial deepening instead of considering the actual corrosion morphology. This means that pittings are simplified by clearly defined geometries, such as spheres. In particular, when pitting corrosion is considered on only one side of the plate, for example, the pitting depth cannot be studied independently of the residual plate thickness or cross-section reduction. A clear distinction between the studied geometric parameters such as corroded volume loss, cross-sectional area, residual thickness, pitting depth, and diameter is therefore not given. Xu and Wang predicted the fatigue life of corroded Q235 steel plates, with finite element models characterised based on 3D profile measurements (Xu and Wang 2015). They concluded that corrosion pits significantly reduce fatigue life.

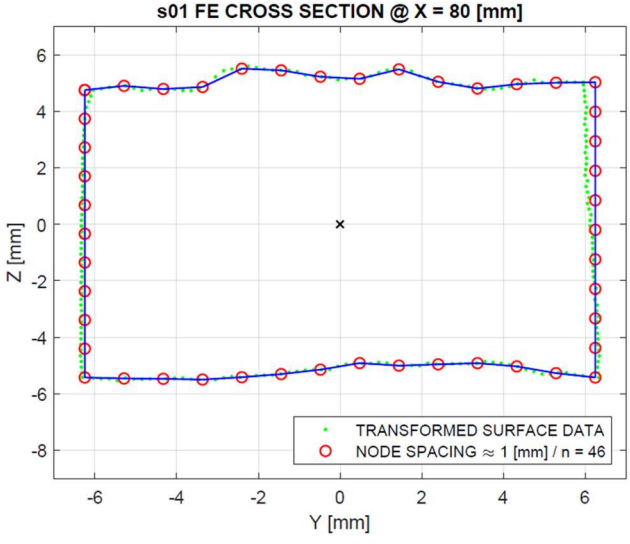

Figure 4. Discretization of finite element cross section. The blue line shows the contour of the modelled cross section (This figure is available in colour online).

We suspect that many previous studies could not simulate pitting corrosion accurately enough, and respective conclusions refer instead to the volume loss and not to the specifics of pitting corrosion. Pitting corrosion is a highly random phenomenon, on the order of magnitude of millimeters. This means that each simplification of the geometry, as well as small inaccuracies while performing experiments, could potentially lead to wrong conclusions, depending on the simplification technique and the specific application. For example, while detailed local pit morphology might not significantly impact buckling analysis, it could be critical for tensile failure analysis, depending on the ductility of the material. The aim of the present contribution is to provide a finite element modeling approach, highlighting several different aspects that improve the accuracy of the numerical simulation of naturally corroded specimens under tensile loading. The models consider as much as possible measurement data (including detailed surface morphology), material properties, global deformations, and experimental tensile test data. However, the analysis of the results of an investigation that can be carried out with such finite element models is not the subject of this article.

The general methods, such as conducting tensile tests and comparing the results with finite element simulations, are well

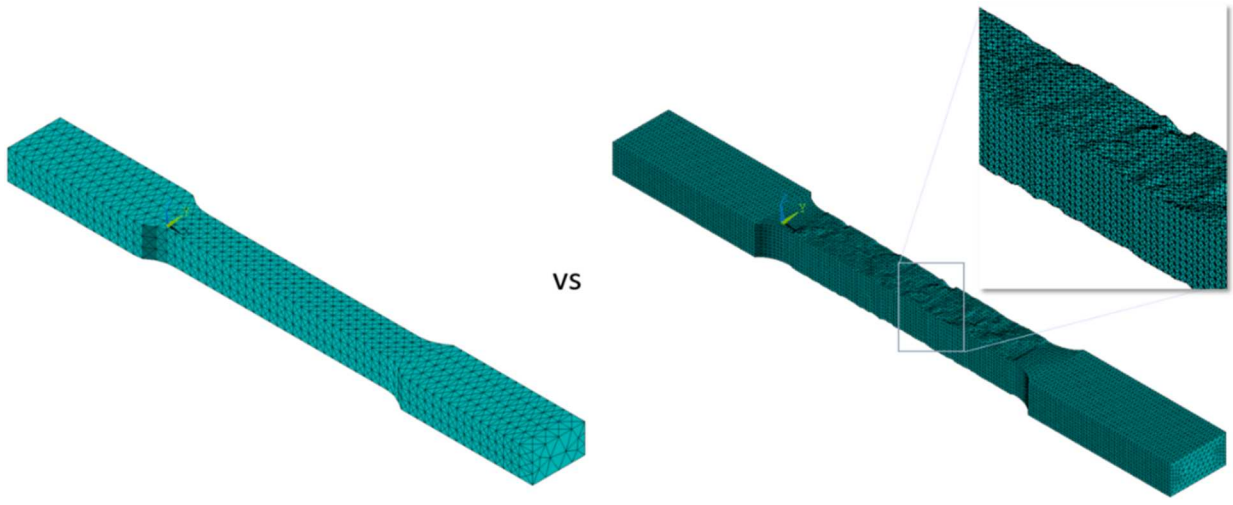

Figure 5. Uniform idealization (left) vs. naturally corroded surface model (right) (This figure is available in colour online).

established. This contribution emphasises the specific modeling requirements needed to accurately investigate the effects of pitting corrosion, which creates random geometries on the millimeter scale and is highly sensitive to even minor inaccuracies in modeling or experimental execution.

2. Methodical approach

The methodical approach is to analyse the geometry of 3D laser scans of naturally corroded specimens and to preprocess them in MATLAB while carrying out parametric finite element simulations based on these specimens. The approach presented is applicable to any kind of tensile test specimens.

First, the laser scanned geometry and the tensile test results are analysed and preprocessed in MATLAB. The resulting geometrical data and strength properties are exported as ASCII files and imported into ANSYS Mechanical. The general approach is shown schematically in Figure 1.

2.1. Data collection: tensile testing and laser scanning of specimens

Naturally corroded specimens were cut from 11 mm (S235) ballast tank steel plates taken from a pipe-laying ship after 30 years of operation. A total of 19 small specimens (s01 – s19, 200 mm total length and 12.5 mm width within 50 mm gauge length) and 17 large specimens (L01 – L17, 450 mm total length and 40.0 mm width within 200 mm gauge length) were prepared according to ASTM E8/E8M-16a (ASTM International 2010) and scanned with a Micro Epsilon LLT2800-25 scanning controller. The variation in size was chosen to explore potential differences in mechanical behaviour, but the corrosion level across all specimens remains consistent. The laser scanning configuration is shown in Figure 2 (Neumann and Ehlers 2019). The top and bottom surfaces were scanned separately and then merged. Based on these surface scans (point clouds), 3D models of each specimen were created, considering the entire volume of corroded specimens. Tensile tests were performed according to ASTM E8/E8M-16a Method C (ASTM International 2010), knowing that care must be taken to ensure that the specimens are free from any conditions that may influence the measured properties (ASTM International 2010), However, the aim of the investigation is to study the effects of pitting morphology, which would therefore not be possible if the surface had been machined, for example. The stress–strain data acquired during the tensile tests as well as the stl files from the scanning process of the specimens were used as the basis for all further investigations and numerical modeling of the corroded specimens. The stl files were converted into xyz-coordinate ASCII files for easier processing in MATLAB.

2.2. Analysis of 3D laser scans and preprocessing of finite element models of naturally corroded specimens with matlab

The philosophy of the MATLAB script was to divide the point cloud (Figure 3) into as many cross sections as possible. Each

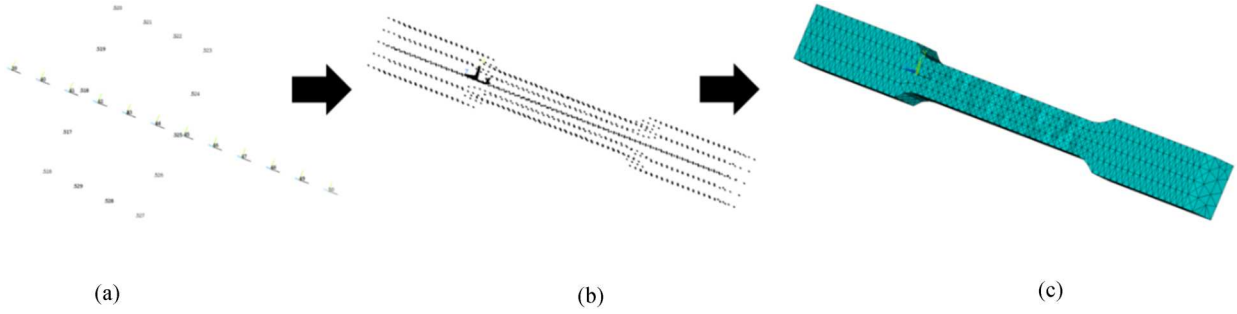

Figure 6. ANSYS modeling approach of corroded tensile test specimens: (a) Centreline definition in global coordinate system, (b) Specimen geometry definition based on key points, (c) Creation of meshed volume (This figure is available in colour online).

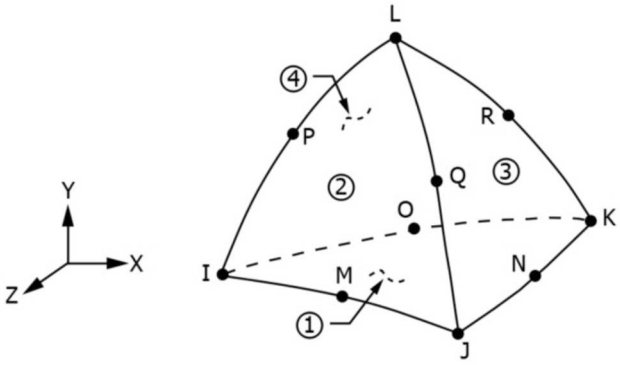

Figure 7. SOLID187 finite element (ANSYS Inc. 2019). The faces of the element are numbered 1-4, each node is marked with a letter (This figure is available in colour online).

cross section was created as follows: A set of points in the cross-section plane was selected. Then, each side of the rectangular cross section was created using a polynomial spline. Equidistant points along the splines were then selected from this total number of points. This controls the surface resolution and ensures that the resolution is the same in the longitudinal and transverse directions. Each cross section was then exactly centred in its local coordinate system by rotating and moving all surface scan points accordingly. The lateral surfaces were simplified by a linear function and it is assumed that the centre of the cross-sectional area is exactly in the middle between the two parallel sides. The cross-sectional area was rotated around the centre point and shifted so that both sides are vertical, so that all points along the respective side lie on the same y-coordinate. The mean distance to the origin of the coordinate system to the upper and lower surfaces was assumed to be the same, which leads to a vertical shift of the cross-section so that the centre point lies at the origin of the coordinates.

Small and large specimen scans, have a varying number of cross sections that were considered within their respective gauge lengths. For the small specimens, in total 398 cross sections were examined within a 50 mm gauge length, resulting in an average cross-sectional spacing of approximately 0.126 mm. In case of the larger specimens with a 200 mm gauge length, 887 cross sections were analysed, leading to an average cross-sectional spacing of approximately 0.225 mm. The scanning speed for the small specimens was 10 mm/s, and doubled for the large specimens (20 mm/s). The respective frequencies were 150 profiles/sec for the small specimens and 125 profiles/sec for the large ones. This was important in order to reduce the total number of scanned profiles and the file size. However, we consider this difference in resolution to be insignificant for the present study, as each specimen was compared to its corresponding finite element model. Therefore, variations in surface scan resolution between specimens have no effect on the conclusions drawn. Additionally, it was found that full scan resolution is unnecessary for accurately simulating the corroded surface morphology. This allowed for finite element models of both specimen types to be created with the same coarser resolution. To control the surface resolution of the finite element models, the cross sections, considered in the finite element analysis were selected out of the total amount of cross sections according to the specified spacing (e.g. 1.0 mm or 0.5 mm), as was the selection of nodes along the overall vertical bending slope, which was calculated beforehand. The specified spacing affects the surface resolution. A smaller distance leads to a finer surface finite element mesh, resulting in a more computationally intensive but more accurate model. The specimens were taken from corroded steel plates that had been in operation for decades and were therefore no longer flat but deformed. As a result, the specimens also showed deformations and were slightly bent in the vertical direction. The bending slope was approximated with a numerical spline through the centre points of each cross section. The cross-section internal nodes describing the shape of the cross section were calculated at an equidistant spacing along each side, equivalent to the defined spacing. Each cross section (e.g. Figure 4) is described by the same number of nodes, which is based on the defined nodal spacing and is essential for the modeling process developed in ANSYS.

Both ends of the specimen followed the same procedure, with the difference that the geometric shape is calculated according to the geometric properties given in the ASTM guideline, and is not based on the surface scans. The thickness of these sections was approximated by the average thickness t_{avg}, of the respective specimen. It was taken into account that the cross section of the actual corroded surface scan started at a consistent coordinate. This position is sufficiently far from the transition radius between the wider clamping areas and the narrow middle section to be studied. This approach has the great advantage that the modelled ends of each specimen are equal (as shown in Figure 5), which facilitates the application of the definition of boundary conditions. In addition, the overall stability is improved significantly because the complicated corroded surface morphology is limited to the gauge length, and the overall number of elements can be reduced.

2.3. Parametric finite element models of naturally corroded specimens with ansys Mechanical

The main purpose of the finite element analysis is to further investigate the effects of nonuniform corrosion on the strength and ductility of steel. One of the most important aspects is to examine the differences between the simplified approach by idealising the corrosion by a uniform surface based on an average thickness t_{avg}, and the more accurate idealisation by considering the scanned, irregular surface morphology, as shown in Figure 5. The investigation of the influence of a uniform idealisation is not possible in the case of the direct analysis of the tensile tests described based on the surface scans only (Biglu et al. 2022). For this, the following possible influences must be isolated and investigated separately:

- Corroded morphology vs. uniform corrosion
- Resolution of the corroded surface morphology
- Global bending shape

For the current application, ANSYS Classic Mechanical is used, because it offers the possibility to create parametric scripts with the ANSYS Parametric Design Language (APDL). With APDL, it is possible to build automated, parametric models by using convenient features like definition of parameters, arrays, macros, looping, and branching. Other commercial finite element software solutions that offer similar functionality, such as LS DYNA, ALTAIR, NASTRAN and ABAQUS, may also be suitable for this application. The modeling approach is optimised to account for the following characteristics:

- Unique surface data sets: The surface morphology of naturally corroded surfaces of each specimen is arbitrary, and does not follow a uniform pattern.
- Large number of different data sets to be processed: In the present example, 32 different laser scans of two kinds of specimens (small and large) with random surface morphologies are processed.

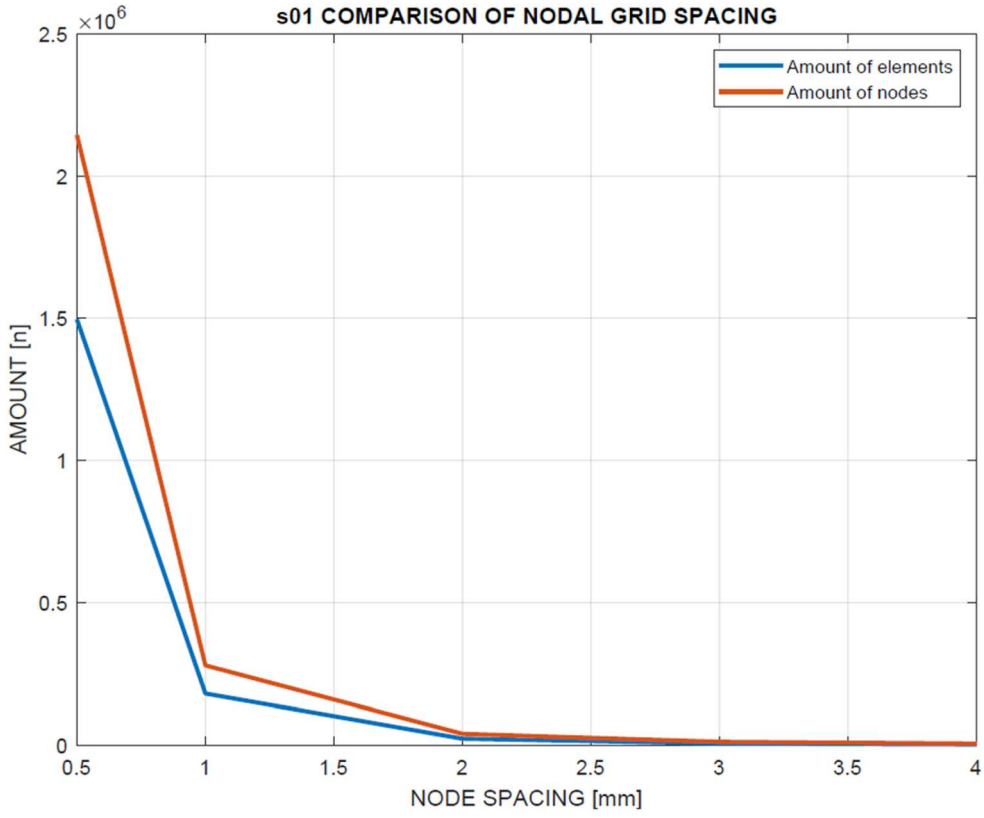

Figure 8. Amount of elements and nodes of a small specimen model for different node spacing.

- Arbitrary vertical and transverse deformations: Each specimen of naturally corroded steel structural members might be deformed randomly, leading to different global bending shapes.

All nodes were exported as x, y, and z coordinates, which were then imported into ANSYS. The process is shown schematically in Figure 6. First, the centreline was created in the global coordinate system by importing the key points along the global bending slope. Then, each cross section was created perpendicular to the centreline based on the local coordinate systems of each key point along the centreline, which led to the geometric representation of the specimen by key points. This method ensures that the entire shape of the specimen can be created from a single casting without any hard transition between the generic ends and the irregular (naturally corroded) centre section. In the next step, the enveloping surface was computed by creating small areas consisting of four key points between all cross sections. For this reason, it was mandatory that all cross sections be composed of the same number of nodes. Finally, the volume was created and meshed based on the enveloping surface.

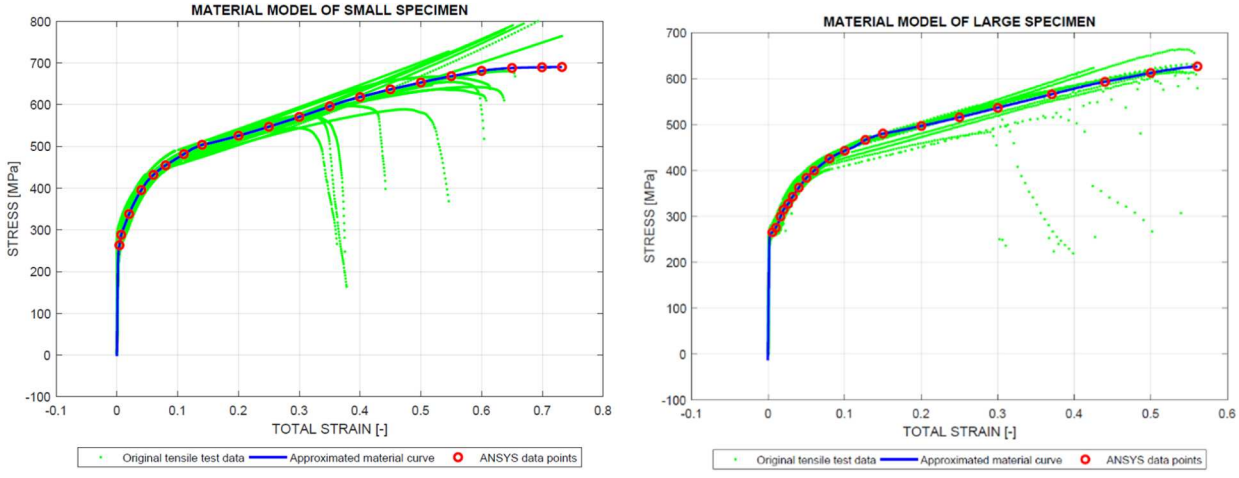

Figure 9. Resulting true stress-strain curves of the material model definition for small and large specimens. The green dots represent the experimental stress strain curves used for curve fitting (This figure is available in colour online).

Table 1. Material properties of corroded specimens.

Type	[kg/dm^3]	t_0 [mm]	E [GPa]	$R_{p0.2}$ [MPa]	σ_m [MPa]	A_{gt} [%]
S235	7.85	11	212	235	360–510	26

2.4. Finite elements

The idealisation of the corroded surface morphology is the main challenge while creating the specimen models. The replication of the exact corroded surface morphology is impossible due to its randomness and complexity with artificial modeling of random pitting corrosion (Wang et al. 2018). Therefore, the aim is to produce the most accurate idealisation of the corroded surfaces possible with reasonable computational effort. To achieve this goal, solid elements are chosen because they are considered more suitable for modeling the detailed surface, which by its nature is highly irregular and contains random pitting (Wang et al. 2018). Plane or shell elements are not applicable in the present case. The surface shapes vary strongly in longitudinal (x), lateral (y) and vertical (z) direction. Therefore, a solid modeling approach was followed, with a meshing strategy that works for all specimens.

The ANSYS SOLID187 structural element was chosen (Figure 7), which is a 10-node, high-order, 3D, tetrahedron element with a quadratic displacement behaviour. This element is suitable for meshing irregular geometries such as those resulting from the corroded surfaces (Appuhamy et al. 2011). Each node has three translational degrees of freedom (x, y, and z directions). In addition, the element considers large deflections and strains, plasticity, creep, hyper elasticity, and stress stiffening (ANSYS Inc. 2019). In general, however, it is advisable to use preferably hexahedrons, or at least quadratic tetrahedrons (with 10 nodes) (Wagner 2017).

The amount of nodes and elements varies with the specified node spacing, as shown for a small specimen model in Figure 8.

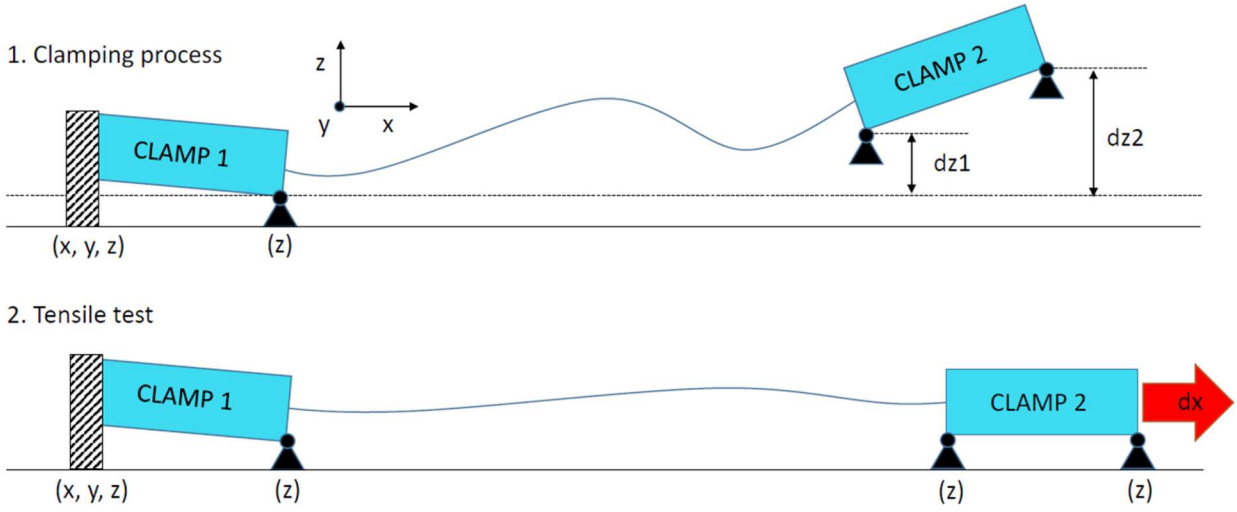

Figure 10. Tensile test simulation load steps. The variables in brackets () are the suppressed degrees of freedom (This figure is available in colour online).

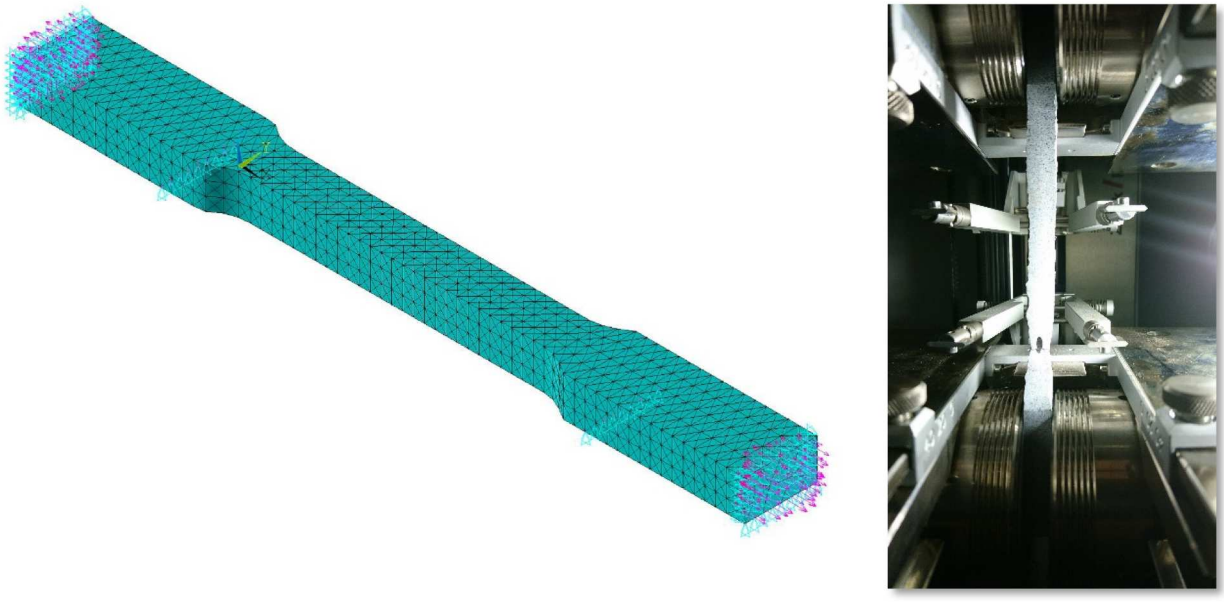

Figure 11. Finite element model with boundary conditions (left) idealising a clamped specimen (right) (This figure is available in colour online).

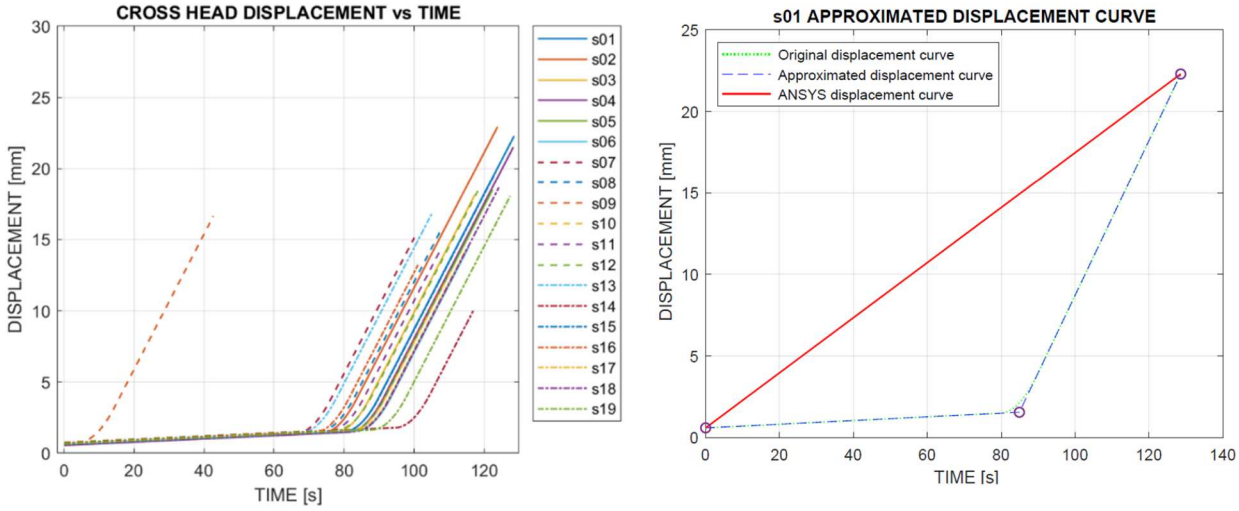

Figure 12. Measured cross-head displacements of small specimens (left) and (right) exemplary linear approximation to be considered within the finite element simulation (This figure is available in colour online).

2.5. Material model

ANSYS Mechanical provides the ability to define a nonlinear material model based on the experimental stress–strain curve. The definition of a nonlinear ANSYS material model is necessary whenever large forces or strains are applied, resulting in plastic stresses above the yield strength. It is therefore necessary to convert engineering stresses and strains into true equivalents, so that plastic and elastic strains can be calculated correctly.

2.5.1. True stress and strain

The formulas are only applicable if the following two conditions are met: First, the material must be incompressible, and second, the stress distribution over the cross sections of the specimen must be uniform. While the first condition is certainly satisfied in the case of S235 steel, the uniform stress distribution over the cross sections may not be satisfied in this case due to randomly distributed pitting corrosion. However, the definition of the plastic behaviour of the material is considered to be sufficiently accurate in this case, and furthermore, it is the most accurate method that can be implemented with the existing data. Unlike nominal stresses, σ_0, and strains, e, true stresses, σ_t (eq. 1), and strains, ϵ_t (eq. 2), take into account the actual cross-sectional area, hence the decrease in cross-sectional area with time at tensile load.

$$\sigma_t = \sigma_0 \cdot (1 + e) = \sigma_0 \cdot exp(\epsilon_t) \tag{1}$$

The true stress is calculated by the natural logarithm of the quotient of the current length over the original length. There is no conversion equation relating engineering to true stress–strain at the time of necking. The equations are only valid until necking occurs. However, it is possible to consider relative strain by approximating cross-sectional reduction instead of elongation, according to eq. 2:

$$\epsilon_t = \begin{cases} \ln\left(\dfrac{\Delta L}{L_0}\right), & \sigma_0 \leq \sigma_m \wedge \ e \leq A_{gt} \\ \ln\left(\dfrac{A_0}{A_k}\right), & \sigma_0 > \sigma_m \ \wedge \ e > A_{gt} \end{cases} \tag{2}$$

$$A_k = A_0 - \sum_{k=1}^{n} dA_k; A_k \in [A_{neck}, A_0] \tag{3}$$

Since the slope of the elongation remains approximately constant after yielding, it is assumed that the increments of cross-sectional reduction, A_k, remain constant until the minimum cross-sectional area due to necking, A_{neck}, is reached, approximately until reaching the ultimate tensile strength σ_m and the respective strain A_{gt}. A_0 and L_0 are the initial cross sectional area and gauge length.

2.5.2. Definition of the material model

Both types of specimens are made from the same type of S235 steel plate. However, a material model for each type of specimen is developed, as the test results are sensitive to the specimen. Material failure (fractures) was not modelled. In general, smaller L_0/A_0 ratios lead to larger elongations (ASTM International 2010).

The resulting true stress–strain curves are shown in Figure 9. The curves were approximated by calculating the curve fit of all measured stress–strain curves from the tensile test. The red circles represent the material data used to define the material model using multilinear isotropic hardening plasticity (MISO) in ANSYS. This means that the material undergoes isotropic hardening, which leads to uniform increase of yield strength in all directions as the material experiences plastic deformations in response to applied loads. The material failure is assessed with the Von Mises or equivalent stress criterion, which indicates potential failure when the equivalent stress exceeds the yield strength. Since Young's modulus, E, is a fundamental property of steel that is not affected by specimen size, a common Young's modulus for both types of specimens is defined, as shown in Table 1. The initial slope of the stress–strain curve is defined by the Young's modulus of the material. The tangent cannot be less than zero or greater than the Young's modulus (ANSYS Inc. 2019).

The true elastic strain, $\epsilon_{el,t}$, and true plastic strain, $\epsilon_{pl,t}$, were calculated according to eqs. 4 and 5 (Truong et al. 2018). Isotropic hardening multilinear material models require the true plastic strain, $\epsilon_{pl,t}$, and the true stresses, σ_t, as inputs. Under this definition, the first stress–strain point corresponds to the yield strength (ANSYS Inc. 2019) and must start at zero plastic strain. Therefore, if the first value is greater than zero, all values must be corrected with $\epsilon_{pl,t,k} = \epsilon_{t,k} - \epsilon_{pl,1}$.

$$\epsilon_{el,t} = \frac{\sigma_t}{E} \tag{4}$$

$$\epsilon_{pl,t} = \epsilon_t - \epsilon_{el,t} \tag{5}$$

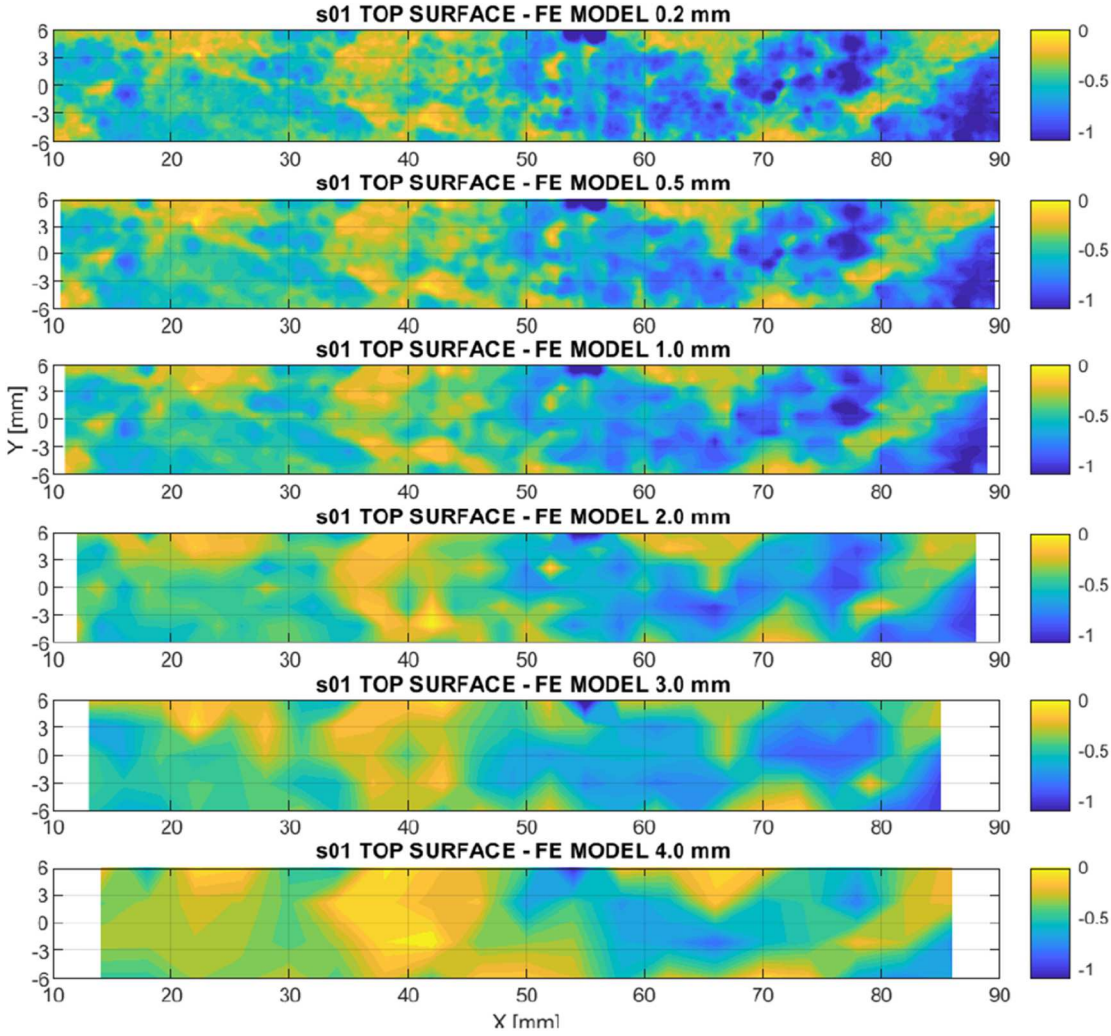

Figure 13. Comparison of different surface resolutions (This figure is available in colour online).

2.6. Simulation of the tensile tests

The goal is to simulate the described tensile tests as accurately as possible, including the clamping process. Two different stages were considered. First, the finite element tensile tests must be able to reproduce the stress–strain curves of the real experiment as accurately as possible. In addition, a common baseline was created, which allows different corrosion idealisations as well as different bending conditions to be simulated without changing the boundary condition loads. The ability to control the simulation environment is a major advantage over performing real experiments, allowing specific effects to be studied while avoiding many unknown influences. For example, the position of the specimen in the testing machine, the application of strain gauges, or the deviation of strain rates influence the results. The simulation of the tensile test itself was divided into two phases, as shown in Figure 9:

- Clamping process: Vertical adjustment of second clamp
- Tensile test: Displacement in longitudinal x-direction

Boundary conditions were applied on the nodes, as shown in Figures 10 and 11. Care was taken to find a combination that would both provide realistic behaviour and not over determine the system, which would increase the difficulty of solving the system of equations. The simulation of the clamping process in the case of a deformed specimen is important to achieve the initial stress level that may result from specimen misalignment. Due to the structure of the model, it is not sufficient to align only the end points. The clamping areas also follow the overall bending shape, so it is necessary to also align the clamping area locally. It should be noted that the numerical model may lead to additional tensile stresses in the grip zones, a condition not observed in the tests. However, due to the sample geometry, larger cross-sections in the grip zone and smaller cross-sections in the gauge length result in higher tensile stresses, leading to tensile deformation primarily within the gauge length. Therefore, it this is considered an acceptable simplification, since it does not change the general behaviour of a tensile test.

Next, the tensile load was applied to that same side of the specimen by defining the longitudinal displacement. The load case was determined by the overall cross-head displacement (in the x-direction) measured during the actual tensile tests, as shown, for example, in Figure 12. However, since a static analysis was performed, the strain rates and time dependence were not considered. Therefore, the displacement was approximated by a linear function. In contrast to the material model definition, each specimen has its own time-displacement curve, as measured during the actual experiment.

Cross-head displacements include the displacements in the clamping system, in the machine itself and the initial sliding of

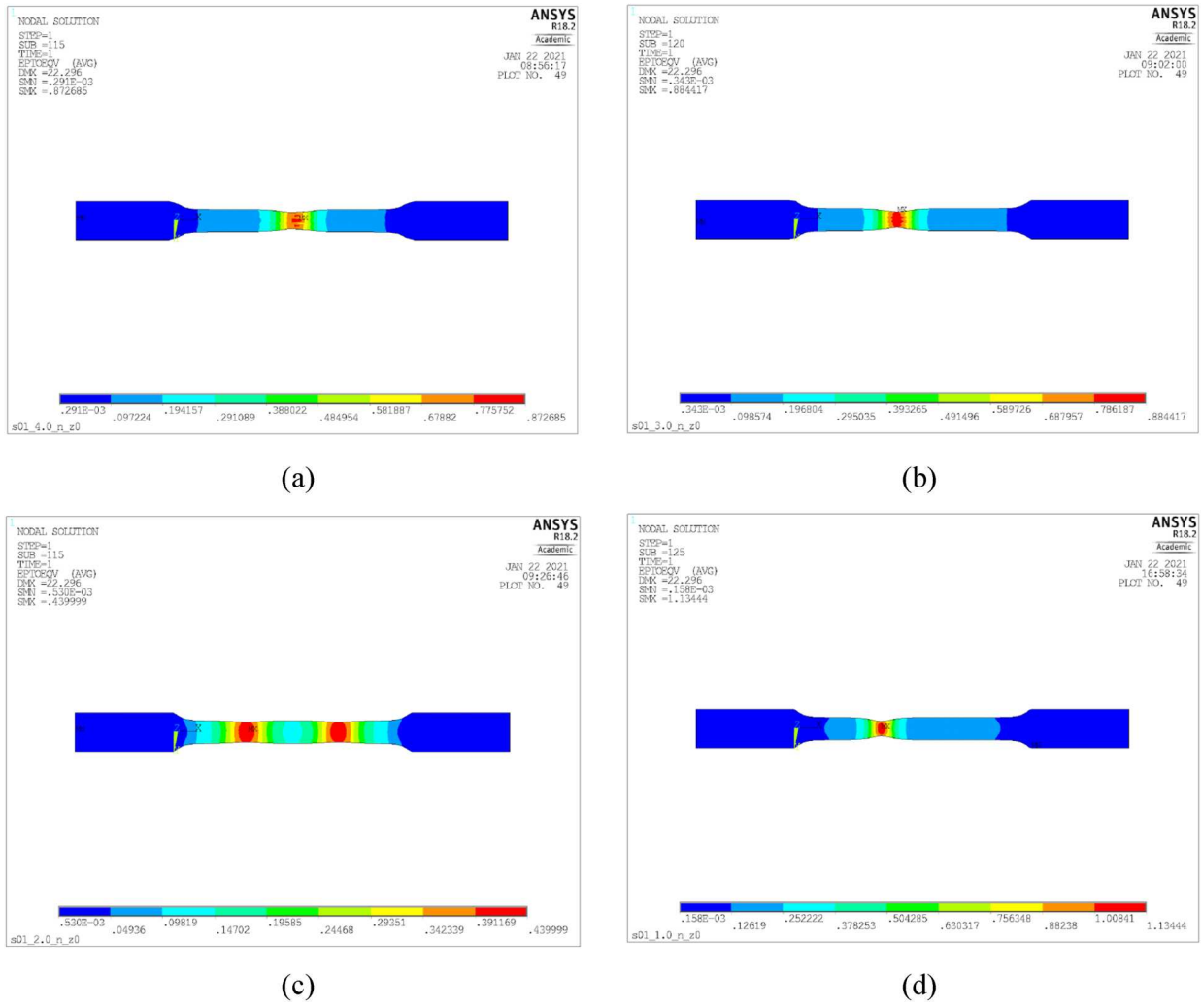

Figure 14. Total strain plots of uniform FEM models of small specimens with 4.0 mm (a), 3.0 mm (b), 2.0 mm (c) and 1.0 mm (d) node spacing (This figure is available in colour online).

the specimen. Consequently, these factors can lead to artificial displacements and consequently to strains to which the specimen is not actually subjected. However, this has no influence in the presented finite element modeling approach.

2.7. Approximation of the corroded surface morphology

Accurate representation of the corroded surface morphology when creating finite element models of actual specimens is one of the key aspects to being able to study the effects of corrosion on strength. Figure 13 shows examples of different resolutions of the same corroded surface, starting with a rough node resolution of 4.0 mm and going up to the highest resolution with a surface node every 0.2 mm.

The discretisation is driven by the resolution of the nodal grid, which determines the level of detail with respect to the morphology of the corroded surface and which has a direct impact on the number of elements and, consequently, on the cost of the calculation. The increase in the number of elements is exponential – for example, increasing the surface resolution from 2 mm to 1 mm in case of a small specimen leads to an increase of the number of elements by factor 4, and by factor 8 increasing the resolution from 1 mm to 0.5 mm. The node density defines the distance between the surface nodes in the three directions (x, y, and z), which allows results in a homogeneous surface grid.

The influence of the resolution of the mesh of a uniform surface was investigated by numerical testing.

Different node spacing were tested: 4.0, 3.0, 2.0 and 1.0 mm. Until the tensile strength was reached, behaviour was basically identical, but changed once necking began. Figure 14 shows that the necking position shifted from the centre to the fully clamped side. The behaviour of the 2.0 mm model is considered erroneous, as two shrinkage positions developed, which is an indicator of numerical errors. This could be caused by convergence issues, when the solution does not converge properly, numerical artifacts can develop, such as multiple shrinkage zones. The most accurate behaviour is achieved by the coarsest (possible) mesh, as it is expected that a symmetrical specimen fails in the middle. A finer mesh does not necessarily lead to more accurate results but increases the risk of numerical errors. For instance, a finer mesh often leads to larger system of equations with more unknowns, which can require more iterations while solving the system of equation and introduce errors into the solution, should the iterative solver not converge properly. Therefore, the nodal resolution and

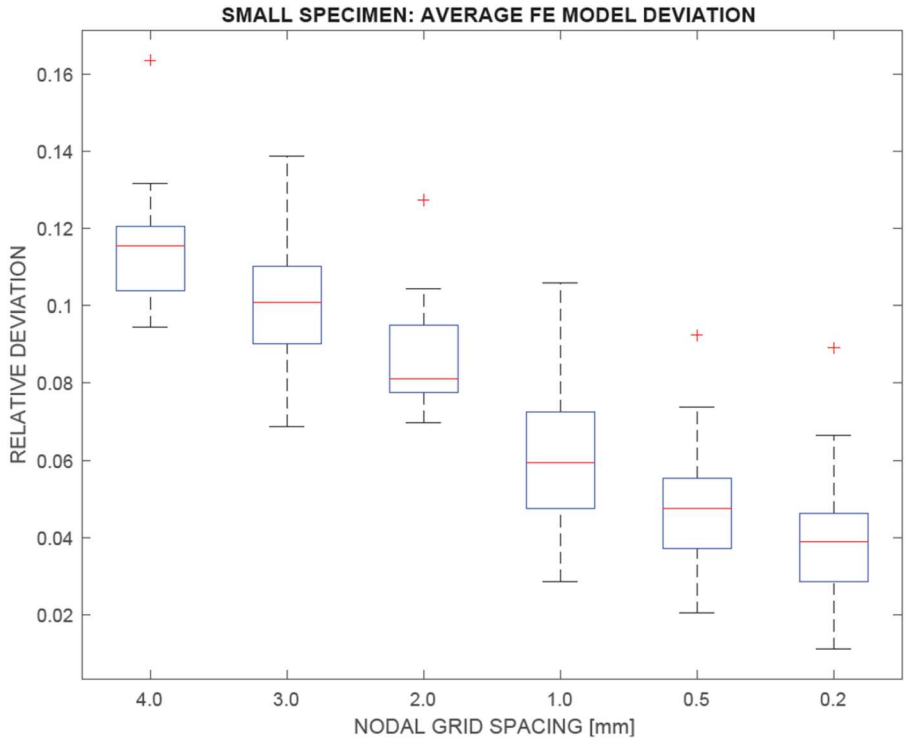

Figure 15. Boxplots of average geometric deviation of finite element models from the original surface scans for different surface resolutions of small specimens. The relative deviation was normalised with the respective value of the geometric parameter of the original surface scan (This figure is available in colour online).

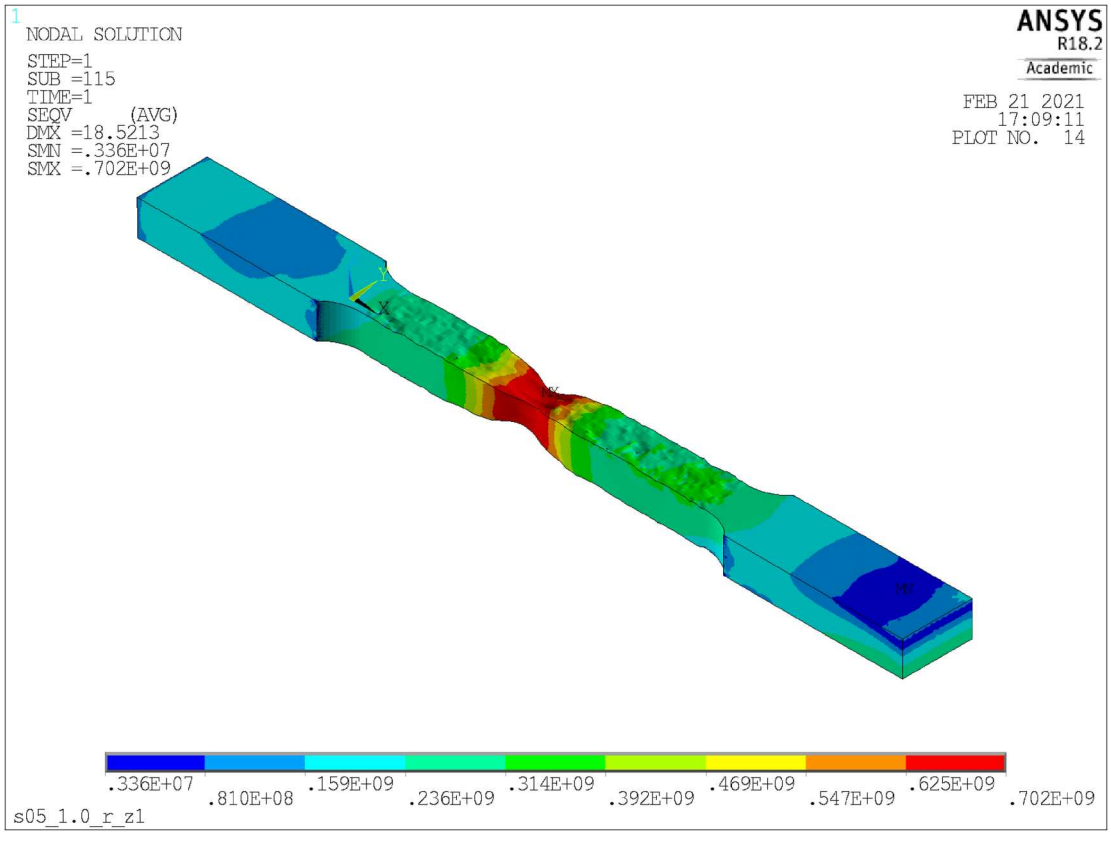

Figure 16. Equivalent stress plot of a small corroded specimen model with 1.0 mm node spacing, considering scanned surface (r) and bending (z1) (This figure is available in colour online).

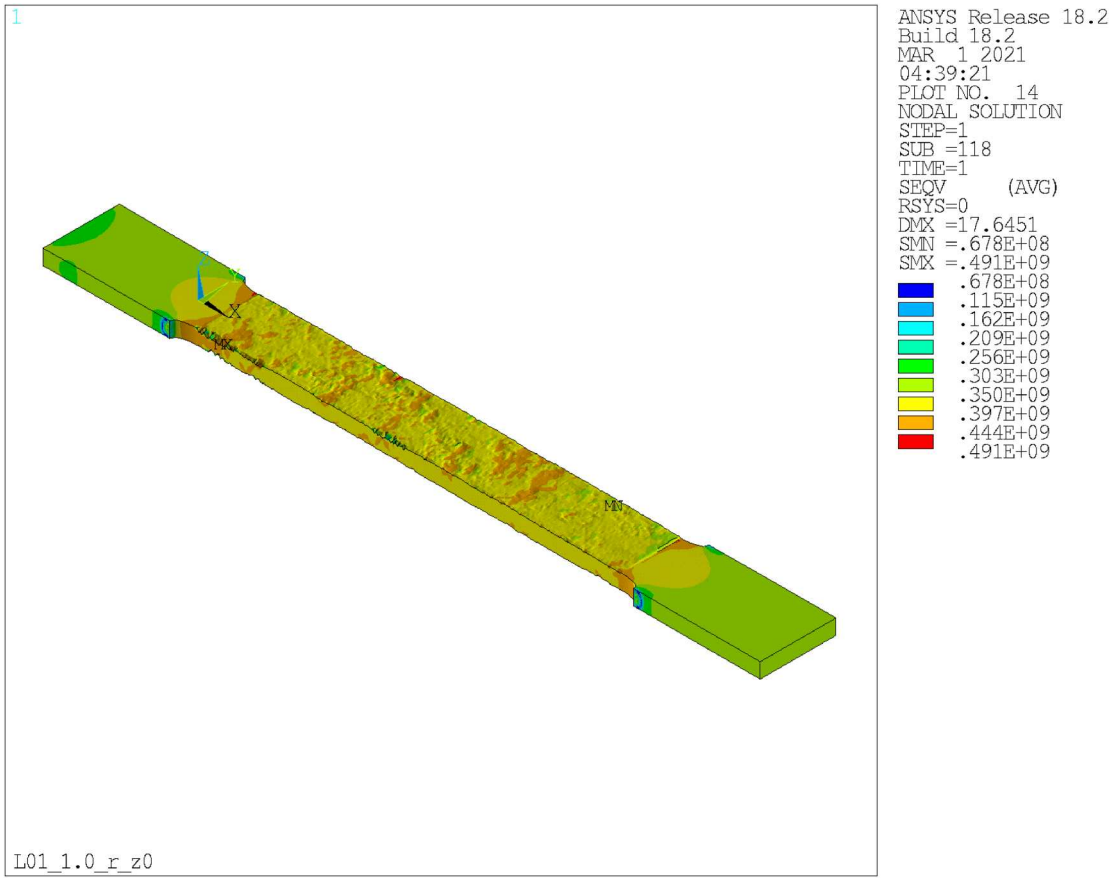

Figure 17. Equivalent stress plot of a large corroded specimen model with 1.0 mm node spacing, considering scanned surface (r) and bending (z1) (This figure is available in colour online).

consequently the element size should be chosen just high enough to represent the surface morphology accurately (Biglu 2022).

Geometrical deviations between the original surface scan and the different nodal grid spacing were assessed and are shown in Figure 15. The average values were calculated based on the deviations of all geometrical parameters to be considered in further analysis of the effects of corrosion, such as minimum cross sectional area, minimum thickness and surface roughness. The selected mesh size based on a nodal grid spacing (resolution) of 1.0 mm is the smallest feasible with respect to computational costs, while it represents the surface geometry accurately.

3. Results & discussion

The results of the finite element modelling approach are compared to the measured data of the experiments. For this purpose, the corroded finite element models with a resolution of 1.0 mm and the vertical bending shape (z1) are considered. Figures 16 and 17 show examples of finite element models of small and large corroded specimens. It should be noted the results are based on the comparison of the resulting stress–strain curves of each specimen, including the ultimate tensile strength,σ_m, the strain at that stage, A_{gt}, and the breaking strain, A_t and the deviation of the experimental fracture position and simulated necking position. The fracture itself was not simulated. The engineering stress–strain curves show a good qualitative match (Figure 18). Figures 19–22 show the box plots of the deviations of the ultimate tensile strength, σ_m, the longitudinal position of the fracture, the total strain at the ultimate tensile strength, A_{gt}, and the total breaking strain, A_t. Apparently, the ultimate tensile strength, R_m (Figure 19), and the longitudinal position of fracture (Figure 20) are accurately predicted by the finite element models. On the other hand, the deviations of the total strains A_{gt} and A_t are higher (Figures 21 and 22).

While the calculation of the ultimate tensile strength, σ_m, is mainly based on the geometric parameters such as the cross-sectional area, the strain behaviour is determined by the defined nonlinear material model. The respective deviations indicate that the material model needs further improvement, which is confirmed by the wide range of deviations. The material model is calculated on the basis of the true stress–strain curves of the samples, which in turn are based on the continuous necking process. Accurate data on the necking process are not available, so material behaviour cannot be improved in the present case. However, this is considered a systematic error in the definition of the finite element models that affects all specimen models equally and does not diminish the validity of investigating geometrical effects of the naturally corroded surface morphology on the stress–strain behaviour in the present case.

As shown in Figure 20, the location of fracture can be reproduced accurately, with a deviation in the range of a few millimeters. It can also be seen that the deviation of the necking location is smaller when the bending shape is taken into account than in the experiment. However, if the bending shape is reversed, e.g. a planar specimen is simulated, the necking location is displaced to the point with the smallest thickness, as expected. This illustrates the superposition of the stresses caused by the bending and thus the importance of considering the global deformation in the simulation. The corresponding equivalent stress plot of that specific

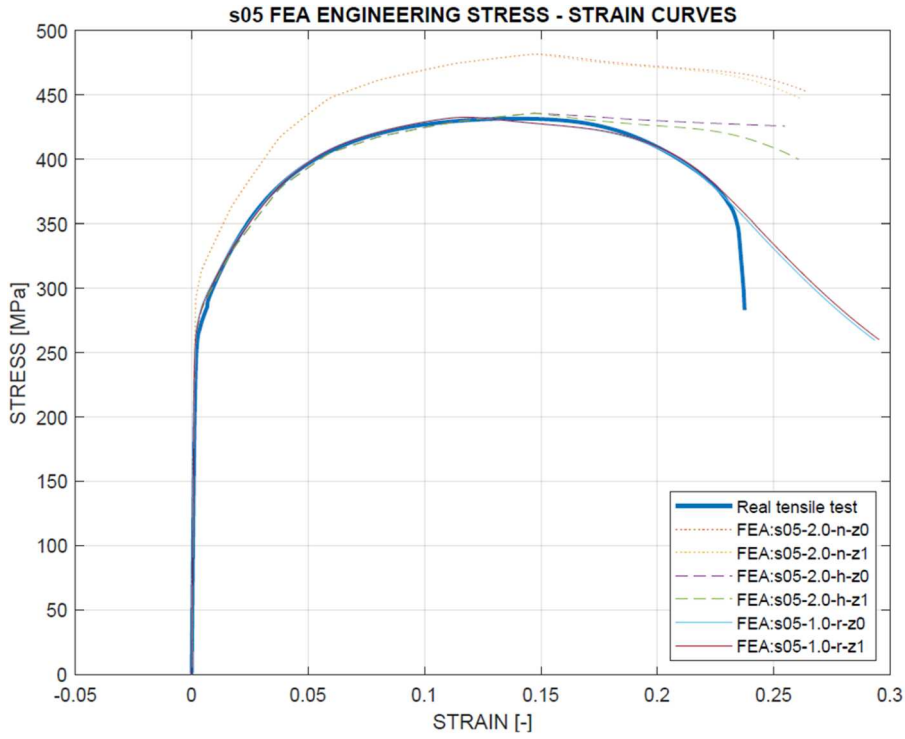

Figure 18. Comparison of finite element stress-strain curves (FEA) with experiment (real tensile test) stress-strain curve (example). There are different types of models of the same specimen, s05: models without corrosion damage (n), models with uniform (h) corrosion, and models that consider the naturally corroded surface morphology (r). In addition, the bending slope is considered (z1) or reversed into a planar condition (z0) (This figure is available in colour online).

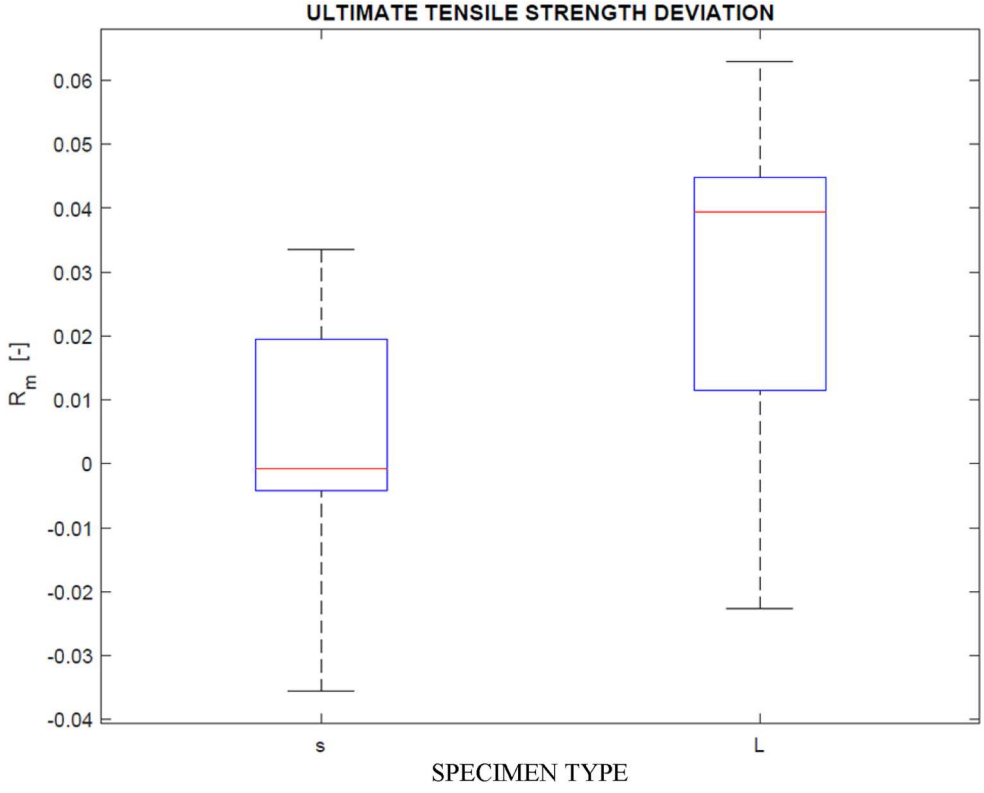

Figure 19. Boxplots of the relative deviation between simulated and experimental ultimate tensile strength σ_m, for both small (s) and large (L) specimens (This figure is available in colour online).

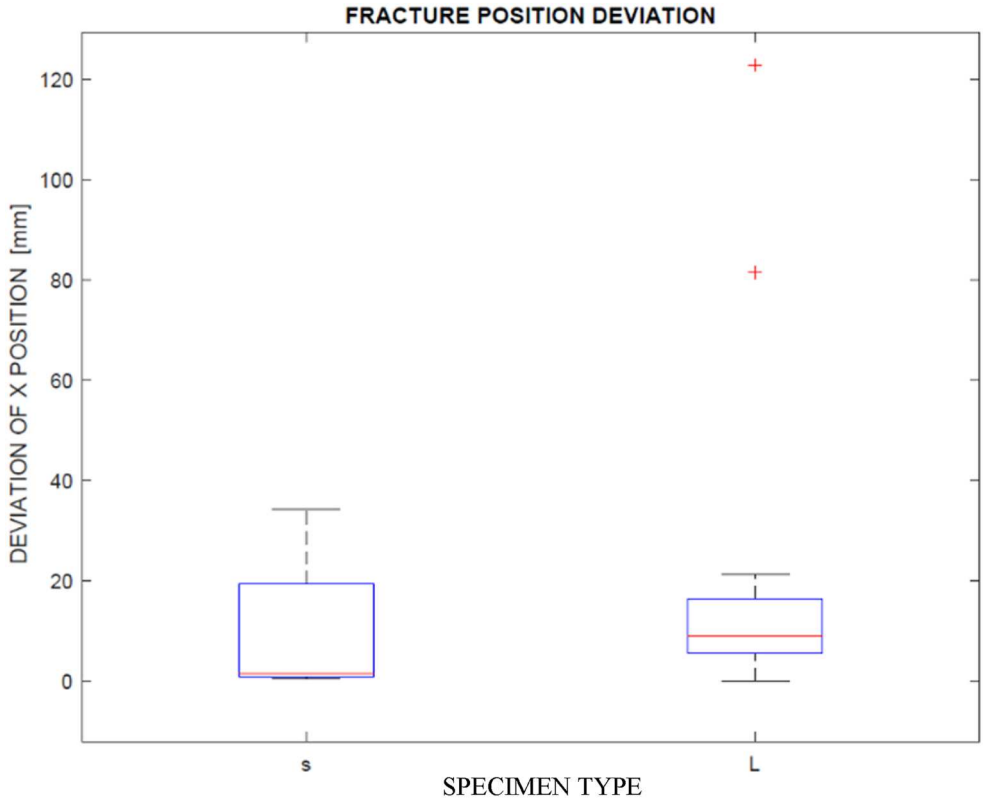

Figure 20. Boxplots of the deviation of simulated and experimental longitudinal fracture position, for both small (s) and large (L) specimens (This figure is available in colour online).

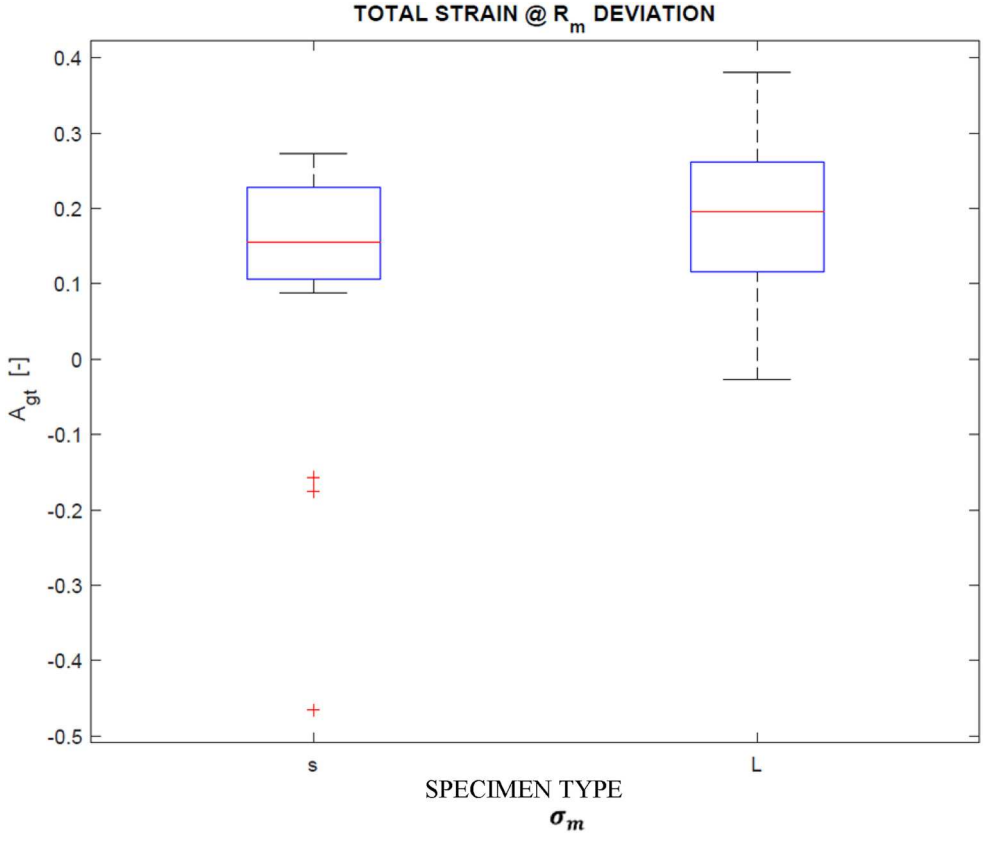

Figure 21. Boxplots of the relative deviation of the simulated and experimental total strain A_{gt} at σ_m, for both small (s) and large (L) specimens (This figure is available in colour online).

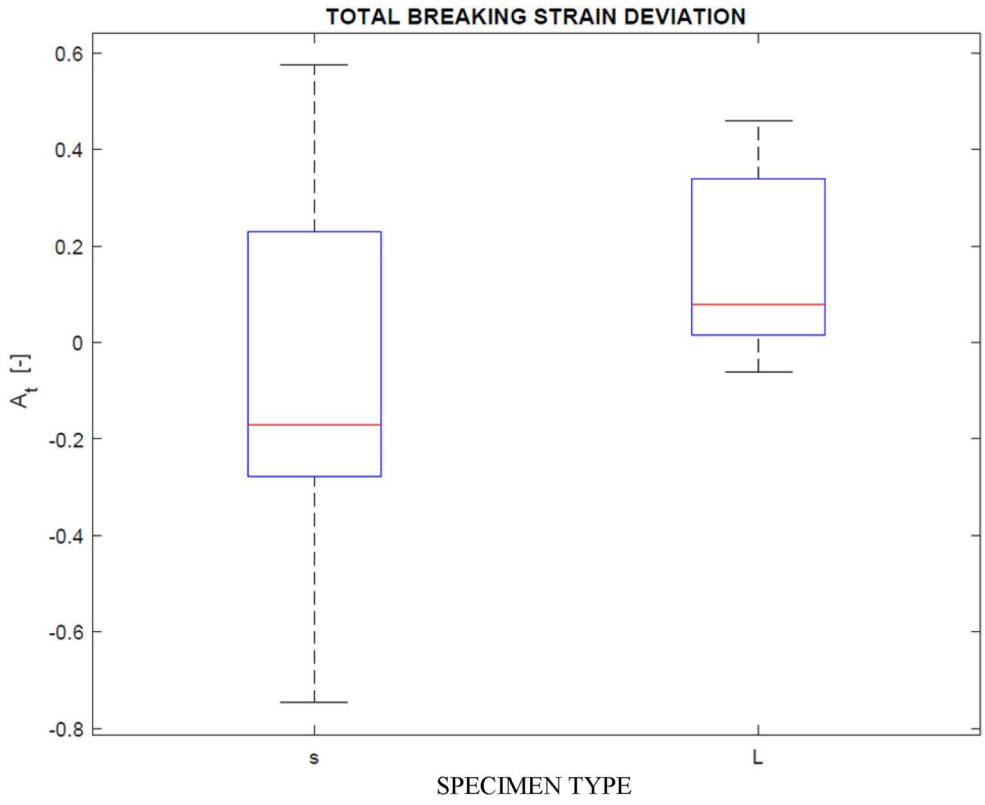

Figure 22. Boxplots of the relative deviation of the simulated and experimental total breaking strain A_t, for both small (s) and large (L) specimens (This figure is available in colour online).

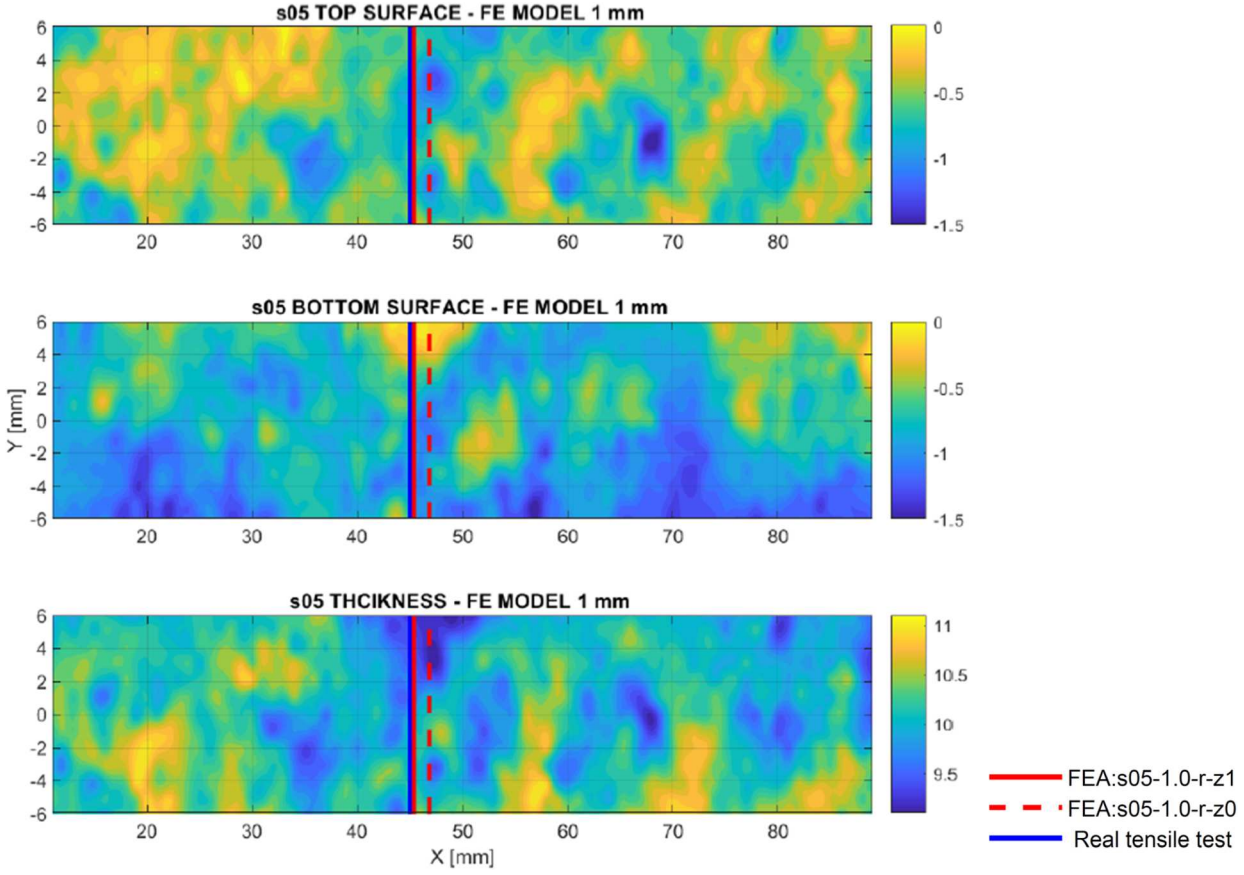

Figure 23. Example of position of simulated necking position compared to the fracture location in a real specimen with the respective finite element model. The blue line represents the location of fracture of the experiment, and the red lines represent the simulated necking locations. The dashed (z0, planar condition) red line deviates from the continuous (z1, bending slope) line, showing the influence of the bending slope (This figure is available in colour online).

finite element model is shown in Figure 16. Furthermore, Figure 23 shows that the bending slope has an influence on the fracture position, due to the induced stresses by the clamps of the tensile test machine. Figure 20 confirms this high accuracy, showing that the median value of the fracture position is approximately 5 mm for small specimens and approximately 10 mm for large specimens.

It was shown that it is possible to accurately simulate tensile tests on naturally corroded specimens using solid finite element models that consider the scanned surface morphology, and that it is necessary to evaluate the strength behaviour of corroded structures. Figure 18 shows that a uniform idealisation of the entire specimen geometry leads to a different stress–strain

behaviour. The full parametric modeling approach turned out to be an efficient way to process a large amount of different specimens (19 small and 17 large specimens). The most important findings that can improve the finite element modeling of corroded structures are listed below:

- To reach an accurate idealisation of a corroded specimen, the whole volume has to be considered, meaning that the consideration of only one corroded surface is not enough. Tetrahedron elements are a suitable option to model the naturally corroded surface morphology.
- A surface resolution of 1 mm is sufficient to simulate the standard monotonic tensile testing of low-carbon steel (S235) when detailed fracture analysis is not of interest. A higher resolution would not necessarily increase the accuracy but would lead to an increase in computational effort and increase the risk of numerical complications.
- The clamping process and global bending shape have an influence on the induced secondary bending stresses, and consequently on the position of necking and fracture, whereby the position can be shifted by several millimeters. This could lead to misleading conclusions when predicting the position of the fracture, which must be considered while scanning corroded specimens to ensure that the bending shape is measured.
- Modeling the corroded surface morphology within the gauge length and idealising both ends of dog-bone-shaped samples has proven to be useful to increase the numerical stability and computational efficiency without compromising the accuracy.
- The definition of the nonlinear material model has a great influence on the material behaviour and must therefore be done carefully. The prediction of the strains is not as accurate as the prediction of the tensile strength, which indicates that the material model can be improved in this case.

4. Conclusion

This study aims to propose an accurate approach for simulating tensile tests on naturally corroded specimens. Based on a detailed analysis of 36 models (19 small and 17 large), it demonstrates that tensile tests on naturally pitting corroded specimens can be effectively and accurately simulated using finite element analysis predicting the location of failure. The simulation results show strong agreement with experimental data, and the modelled corroded surfaces closely replicate actual scanned surfaces. This research highlights several critical aspects for precisely assessing the tensile strength of corroded specimens:

- The naturally corroded volume must be modelled with high accuracy along the entire gauge length, while the ends can be idealised with uniform surfaces. A resolution of at least 1 mm is required for idealising the surface morphology when simulating standard monotonic tensile tests on low-carbon steel (S235) upon the onset of actual fracture. The latter is not within the scope of this research.
- Specimen deformation, particularly global bending during the clamping process, has a significant impact on tensile test behaviour. Secondary bending stresses can shift the necking and fracture locations by several millimeters, and must be carefully considered to ensure accurate and reliable results.
- The presented method allows a close agreement between numerical and experimental results. it is emphasised that the high agreement is established by the geometric modeling, but not through altering basic material properties.
- Artificial pittings fail to replicate the complex behaviour of naturally occurring pitting corrosion, as they produce incorrect surface stress distributions that can cause fracture to initiate at incorrect locations. Surface stress distributions caused by the corroded pitting defects are governing the failure. Consequently, artificially introduced pittings fail replicating the complex behaviour of naturally occurring pitting.

The study also finds that overlooking these modeling criteria can introduce substantial inaccuracies, potentially skewing interpretations of corrosion's impact on material performance. Importing geometry point clouds directly into finite element software, for example, may not be ideal due to potential data discrepancies that can influence simulation outcomes.

Key variables like pitting depth, typically on the millimeter scale, can be overshadowed by secondary effects like bending shape, which can lead to deviations on the order of several times larger than the pitting depth. This highlights that the bending shape can displace necking and fracture by millimeters or even centimeters, masking the true effects of corrosion morphology. Therefore, simplified or artificial pitting shapes are insufficient for accurately representing the complex influence of natural pitting corrosion, and high-resolution, realistic surface modeling is crucial for reliable insights into corrosion behaviour.

These findings have significant implications for existing construction standards and guidelines, where corrosion is frequently assumed to cause uniform material degradation. This assumption fails to capture the real-world complexity of corrosion processes, potentially leading to misinterpretations of structural integrity and inaccuracies in estimating the energy absorption capacity of corroded structures. It is recommended that the assumptions made in current guidelines be reassessed to ensure they account for the intricate effects of pitting corrosion and that current safety factors are sufficiently robust to cover the broader implications of these findings.

Acknowledgements

Our special thanks goes to Karoline Neumann for planning and carrying out all works related to the corroded specimens, the tensile tests and creating the data basis on which these finite element models are based. Part of the content and figures are based on the corresponding author's doctoral thesis on the "Effects of corrosion on the local behavior of steel structures under tensile loading" (Biglu 2022).

Disclosure statement

No potential conflict of interest was reported by the author(s).

Funding

This work was authored in part by the National Renewable Energy Laboratory, operated by Alliance for Sustainable Energy, LLC, for the U.S. Department of Energy (DOE) under Contract No. DE-AC36-08GO28308. Funding provided by the Wind Energy Technologies Office. The views expressed in the article do not necessarily represent the views of the DOE or the U.S. Government. The U.S. Government retains and the publisher, by accepting the article for publication, acknowledges that the U.S. Government retains a nonexclusive, paid-up, irrevocable, worldwide license to publish or reproduce the published form of this work, or allow others to do so, for U.S. Government purposes.

Data availability statement

The data is available on request.

ORCID

Franz von Bock und Polach http://orcid.org/0000-0002-4093-8381

References

Ahmad RR. 2012. Plastic collapse load of corroded steel plates. Sadhana - Academy Proceedings in Engineering Sciences. 37(3):341–349.

Ahmmad MM, Sumi Y. 2010. Strength and deformability of corroded steel plates under quasi-static tensile load. J Mar Sci Technol. 15(1):1–15.

ANSYS Inc. 2019. ANSYS Inc. PDF Documentation for Release 2020 R1 [online]. Available from: https://d.shikey.com/down/Ansys.Products.2020.R1.x64/install_docs/Ansys.Products.PDF.Docs.2020R1/readme.html [Accessed 13 Mar 2022].

Appuhamy JMRS, Kaita T, Ohga M, Fujii K. 2011a. Prediction of residual strength of corroded tensile steel plates. International Journal of Steel Structures. 11(1):65–79.

Appuhamy JMRS, Ohga M, Kaita T, Dissanayake R. 2011b. Reduction of ultimate strength due to corrosion -A finite element computational method. Int J Eng. 5(2):194–207.

ASTM International 2010. ASTM e8/E8M - 16a standard test methods for tension testing of metallic materials. *Annual Book of ASTM Standards 4*, 1–27.

Biglu M. 2022. *Effects of corrosion on the local behavior of steel structures under tensile loading*. Hamburg: Schriftenreihe Schiffbau.

Biglu, M., von Bock und Polach, F., and Ehlers, S., 2022. New Findings on the Impact of the Idealization of Corrosion on the Brittle Failure of Steel. *Proceedings of the International Conference on Offshore Mechanics and Arctic Engineering - OMAE*. 1–7.

Garbatov Y, Guedes Soares C, Parunov J, Kodvanj J. 2014. Tensile strength assessment of corroded small scale specimens. Corros Sci. 85:296–303.

Garbatov Y, Parunov J, Kodvanj J, Saad-Eldeen S, Soares CG. 2016. Experimental assessment of tensile strength of corroded steel specimens subjected to sandblast and sandpaper cleaning. Marine Structures. 49:18–30.

Garbatov Y, Saad-Eldeen S, Guedes Soares C, Parunov J, Kodvanj J. 2019. Tensile test analysis of corroded cleaned aged steel specimens. Corrosion Engineering Science and Technology. 54(2):154–162.

Garbatov Y, Soares CG, Parunov J, Kodvanj J. 2014. Tensile strength assessment of corroded small scale specimens. Corros Sci. 85:296–303.

IACS, 2023a. CSR - Common Structural Rules for Bulk Carriers and Oil Tankers, 822.

IACS 2023b. URZ Requirements concerning SURVEY AND CERTIFICATION, 857.

Kainuma S, Jeong YS, Ahn JH. 2014. Investigation on the stress concentration effect at the corroded surface achieved by atmospheric exposure test. Mater Sci Eng A. 602:89–97.

Kaita T, Appuhamy JMRS, Itogawa K, Ohga M, Fujii K. 2011. Experimental study on remaining strength estimation of corroded wide steel plates under tensile force. Procedia Eng. 14:2707–2713.

Kariya, A. ; Tagaya, K. ; Kaita, T. ; Fuji i, K.., 2005. Mechanical properties of corroded steel plate under tensile force [online]. *Proceedings of the 3rd International Structural Engineering and Construction Conference (ISEC-03)*. Available from: https://www.researchgate.net/publication/288346202_Mechanical_properties_of_corroded_steel_plate_under_tensile_force [Accessed 26 Mar 2022].

Kim IT, Dao DK, Jeong YS, Huh J, Ahn JH. 2017. Effect of corrosion on the tension behavior of painted structural steel members. J Constr Steel Res. 133:256–268.

Melchers RE. 2008. Extreme value statistics and long-term marine pitting corrosion of steel. Probab Eng Mech. 23(4):482–488.

Nakai T, Matsushita H, Yamamoto N, Arai H. 2004. Effect of pitting corrosion on local strength of hold frames of bulk carriers (1st report). ARTICLE IN PRESS. *Marine Structures*. 17:403–432.

Neumann KM, Ehlers S. 2019. Power spectrum for surface description of corroded ship structure from laser scan. Proceedings of the ASME 2019 38th International Conference on Ocean, Offshore and Arctic Engineering. Volume 3: Structures, Safety, and Reliability; June 9–14; Glasgow, Scotland, UK; ASME. https://doi.org/10.1115/OMAE2019-95907.

Paik JK, Lee JM, Ko MJ. 2003. Ultimate compressive strength of plate elements with pit corrosion wastage. Proceedings of the Institution of Mechanical Engineers, Part M: Journal of Engineering for the Maritime Environment. 217(4):185–200.

Paik JK, Lee JM, Ko MJ. 2004. Ultimate shear strength of plate elements with pit corrosion wastage. Thin-Walled Struct. 42(8):1161–1176.

Paik JK, Lee JM, Park Y, Hwang JS, Kim CW. 2003. Time-variant ultimate longitudinal strength of corroded bulk carriers. Marine Structures. 16(8):567–600.

Park SH, Lee SM, Yu Y, Cho SR. 2024. Residual strength of corroded ring-stiffened cylinder structures under external hydrostatic pressure. International Journal of Naval Architecture and Ocean Engineering. 16:100590.

Rahbar-Ranji A. 2012. Ultimate strength of corroded steel plates with irregular surfaces under in-plane compression. Ocean Eng. 54:261–269.

Rahbar-Ranji A, Niamir N, Zarookian A. 2015. Ultimate strength of stiffened plates with pitting corrosion. International Journal of Naval Architecture and Ocean Engineering. 7(3):509–525.

Saad-Eldeen S, Garbatov Y, Guedes Soares C. 2011a. Corrosion-dependent ultimate strength assessment of aged box girders based on experimental results. Transactions - Society of Naval Architects and Marine Engineers. 119(4):591–602.

Saad-Eldeen S, Garbatov Y, Soares CG. 2011b. Experimental assessment of the ultimate strength of a box girder subjected to severe corrosion. Marine Structures. 24(4):338–357.

Tekgoz M, Garbatov Y, Soares CG. 2020. Review of ultimate strength assessment of ageing and damaged ship structures. J Mar Sci Appl. 19(4):512–533.

Truong DD, Shin HK, Cho SR. 2018. Repeated lateral impacts on steel grillage structures at room and sub-zero temperatures. Int J Impact Eng. 113:40–53.

Wagner M. 2017. *Lineare und nichtlineare FEM*. Regensburg: Springer Vieweg Wiesbaden.

Wang R, Shenoi RA, Sobey AJ. 2018. Ultimate strength assessment of plated steel structures with random pitting corrosion damage. J Constr Steel Res. 143:331–342.

Wang Y, Xu S, Wang H, Li A. 2017. Predicting the residual strength and deformability of corroded steel plate based on the corrosion morphology. Constr Build Mater. 152:777–793.

Xu SH, Wang YD. 2015. Estimating the effects of corrosion pits on the fatigue life of steel plate based on the 3D profile. Int J Fatigue. 72:27–41.

Yao Y, Yang Y, He Z, Wang Y. 2018. Experimental study on generalized constitutive model of hull structural plate with multi-parameter pitting corrosion. Ocean Eng. 170:407–415.

Zhang Y, Huang Y, Wei Y. 2017. Ultimate strength experiment of hull structural plate with pitting corrosion damage under unaxial compression. Ocean Eng. 130:103–114.

Zhang Y, Huang Y, Zhang Q, Liu G. 2016. Ultimate strength of hull structural plate with pitting corrosion damnification under combined loading. Ocean Eng. 116:273–285.